CARS-based silicon photonics

Nathalie Vermeulen, Christof Debaes, Hugo Thienpont
Dept. of Applied Physics and Photonics, Vrije Universiteit Brussel, Brussels, Belgium

ABSTRACT

In this invited paper, we will first discuss the recent research progress regarding silicon-on-insulator (SOI) Raman wavelength converters, the working principle of which is based on the four-wave mixing process of coherent anti-Stokes Raman scattering (CARS). Next, we will present our research results on other aspects of CARS in SOI waveguides. First, starting from the basic formalism for CARS we will show that, in contrast to what most scientists believe, CARS exchanges energy with the Raman medium in which it takes place and is even able to extract energy (i.e. extract phonons) from it. Furthermore, we will introduce a novel CARS-based approach to reduce the heat dissipation in Raman lasers due to the quantum defect between pump and lasing photons, and we will numerically demonstrate that with this "CARS-based heat mitigation technique" the quantum-defect heating in SOI waveguide Raman lasers could be reduced with as much as 35%.

Keywords: silicon-on-insulator, Coherent Anti-Stokes Raman Scattering, Raman lasers, heat mitigation

1. INTRODUCTION

Silicon is a material that is of great importance not only to the electronics industry but since a few years also to the field of photonics. Especially photonic devices based on the "silicon-on-insulator" (SOI) material system have the advantage that they can be integrated with silicon-based electronic components and that they can be fabricated using the high-precision CMOS mass-manufacturing technologies. Furthermore, the large refractive index difference in SOI structures establishes a strong confinement of the light, which enables extensive component miniaturization and facilitates the exploitation of nonlinear optical effects in these structures.

Silicon itself is a highly nonlinear optical material that features a high third-order Kerr nonlinearity and an even larger third-order Raman susceptibility. During a Raman scattering interaction in silicon, incident photons are scattered on a thermal vibration of the silicon crystal lattice, so that new photons with a different energy and wavelength are generated. The most important, non-spontaneous Raman processes are stimulated Stokes Raman scattering (SSRS), coherent anti-Stokes Raman scattering (CARS), and stimulated anti-Stokes Raman scattering (SARS), which in practice all occur simultaneously albeit with different efficiencies.[1] In the absence of population inversion between the involved oscillation energy level $|f\rangle$ and the ground energy level $|i\rangle$ of the Raman-active medium under consideration, SSRS – in many cases the strongest Raman process – converts pump photons to lower-energy Stokes photons while generating phonons in the medium (see Figure 1(a)). This process is responsible for both the lasing action in Raman lasers and the light amplification in Raman amplifiers, and both types of Raman devices have been successfully demonstrated in SOI technology.[2,3,4] Besides lower-energy Stokes photons, also higher-energy anti-Stokes photons can be generated in a Raman medium through the process of CARS, but part of these higher-energy photons will be converted back to pump photons by SARS; a process which, like SSRS, is accompanied by the creation of phonons (see Figure 1(b)). How exactly these anti-Stokes photons are generated by CARS will be discussed further on in this paper.

CARS is a unique Raman mechanism in the sense that it is not only a Raman-resonant interaction but also a four-wave mixing process. Due to the resonant and coherent nature of this four-wave mixing mechanism, CARS has not only become one of the most important optical analysis tools in the domains of spectroscopy and microscopy,[5,6] but has also proven to be an efficient wavelength conversion mechanism for so-called anti-Stokes Raman converters turning a coherent Stokes input signal into a coherent anti-Stokes output signal. Also for realizing anti-Stokes Raman converters one can make use of SOI waveguides as Raman-active medium.[7,8,9]

In this paper, we will first discuss the recent progress on highly-efficient CARS-based wavelength conversion in SOI technology. Next, we will present our research results on other aspects of CARS in SOI waveguides. First, starting from the basic formalism for CARS, we will show that the physical nature of this four-wave mixing process should be interpreted in a different way than is commonly assumed. More specifically, we will demonstrate that, in contrast to what most scientists

Photonic Materials, Devices, and Applications III, edited by Ali Serpengüzel, Gonçal Badenes, Giancarlo C. Righini,
Proc. of SPIE Vol. 7366, 736603 · © 2009 SPIE · CCC code: 0277-786X/09/$18 · doi: 10.1117/12.822100

believe, CARS exchanges energy with the Raman medium in which it takes place and is even able to extract energy (i.e. extract phonons) from it. Furthermore, we will introduce a novel approach where CARS is used to reduce the heat dissipation in Raman lasers due to the quantum defect between pump and lasing photons, and we will numerically demonstrate that with this "CARS-based heat mitigation technique" the quantum-defect heating in SOI waveguide Raman lasers could be reduced with as much as 35%.

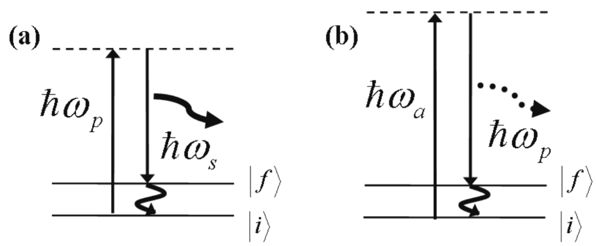

Fig. 1. Schematic representation of (a) stimulated Stokes Raman scattering (SSRS) and (b) stimulated anti-Stokes Raman scattering (SARS) in a non-inverted Raman medium.

2. RECENT PROGRESS REGARDING CONVERSION EFFICIENCY OF RAMAN WAVELENGTH CONVERTERS IN SOI TECHNOLOGY

So far, most research on SOI Raman converters has been carried out by the group of Jalali *et al.*. Apart from modeling the operation of an SOI Raman converter,[7,8] they have carried out several experiments to investigate the attainable conversion efficiencies. In their initial experiments, the conversion efficiency (i.e. the ratio of the anti-Stokes output to the Stokes input) was only of the order of magnitude of 10^{-5}, because the operation conditions of the SOI converter were not optimal.[7,8] More specifically, the SOI waveguide featured a large phase mismatch for CARS, and rather than using a high-peak-power pulsed source they employed a continuous-wave laser for pumping, which further reduced the efficiency of the nonlinear CARS process. However, in 2008 the group of Jalali *et al.* showed that when using high-peak-power pump pulses, one can establish very high conversion efficiencies of 0.5 and more, even in case the SOI waveguide under consideration features a large phase mismatch.[9] In addition, they demonstrated in 2008 a technique where the phase mismatch of CARS is tuned close to zero by electrically tuning the waveguide birefringence.[10] In conclusion, there are very promising perspectives for practical and efficient SOI-based Raman converters, and the application potentialities of these devices in a.o. the telecom domain will be further extended accordingly.

In spite of the research progress regarding the wavelength conversion capabilities of CARS, the actual nature and behavior of this process in Raman converters has not been properly described so far. Our approach to solve this issue will be presented in the following Section.

3. BEHAVIOR OF CARS IN RAMAN WAVELENGTH CONVERTERS OPERATING AT EXACT RAMAN RESONANCE

3.1 Introduction

Although it is well known that CARS has many potentialities for establishing wavelength conversion (see Sec. 2), the nature and behavior of this process in Raman converters has not been properly described so far. Today it is well understood and fully accepted by the scientific community that CARS is a four-wave mixing process involving two pump photons, one Stokes photon and one anti-Stokes photon, and that the wave vectors of the photons $k_{\{p,s,a\}} = n_{\{p,s,a\}}\omega_{\{p,s,a\}}c^{-1}$, where $\omega_{\{p,s,a\}}$ and $n_{\{p,s,a\}}$ represent the pump, Stokes and anti-Stokes angular frequencies and refractive indices, respectively, are phase-matched if $\overrightarrow{\Delta k} = 2\overrightarrow{k_p} - \overrightarrow{k_s} - \overrightarrow{k_a} = \vec{0}$ (see Figure 2(a)). However, for CARS in a Raman converter operating at exact Raman resonance (i.e. the most common working point for Raman lasers, amplifiers and converters), a full description which clarifies how exactly these four photons interact in the process along the converter path length is still lacking.

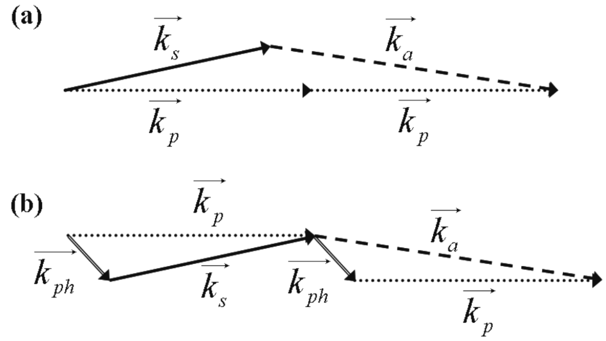

Fig. 2. Schematic representations of the phase matching condition for CARS. (a) Scheme of the well established phase matching condition $\overrightarrow{\Delta k} = 2\overrightarrow{k_p} - \overrightarrow{k_s} - \overrightarrow{k_a} = \vec{0}$. (b) Phase matching condition for the CARS process of Fig. 3(a), which essentially corresponds to the phase matching condition of Fig. 2(a).

In this Section, we present a model that fully describes the quasi-stationary behavior of CARS in an anti-Stokes Raman converter operating at exact Raman resonance.[13] Our model explains the CARS behavior as a function of two key parameters; namely the phase mismatch Δk of the four-wave mixing process and the level of pump depletion. For the case of negligible pump depletion, we show that, whatever the value of the phase mismatch, the CARS process will convert a Stokes photon and a pump photon to an anti-Stokes photon and a pump photon while annihilating two phonons in the Raman medium. This is schematically represented in Figure 3(a). Also in case the pump gets depleted and the phase mismatch is small, CARS will act in this way. We remark that the thus annihilated phonons are coherent phonons which were generated earlier by SSRS, and that in the CARS wave vector diagram corresponding to Figure 3(a) (with phonon wave vectors $\overrightarrow{k_{ph}}$ included) phase matching is still obtained for photon wave vectors satisfying the condition $\overrightarrow{\Delta k} = 2\overrightarrow{k_p} - \overrightarrow{k_s} - \overrightarrow{k_a} = \vec{0}$ (see Figure 2(b)). Next, in case pump depletion occurs in combination with a considerable phase mismatch, we find that CARS will switch over from the interaction type depicted in Figure 3(a) to the reverse interaction type shown in Figure 3(b). Hereby, an anti-Stokes photon and a pump photon are converted to a Stokes photon and a pump photon, and phonons are created in the medium. We remark that the thus created phonons are again coherent phonons. Finally, besides presenting our new model for CARS at exact Raman resonance, we discuss in this Section the fundamental differences between our CARS theory and the earlier presented interpretations of the CARS process.

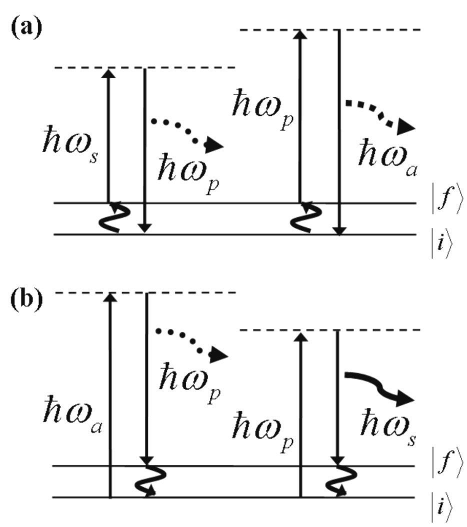

Fig. 3. Schematic representation of (a) CARS in case it converts a Stokes photon and a pump photon to an anti-Stokes photon and a pump photon, while annihilating two phonons in the medium; (b) CARS in case it converts an anti-Stokes photon and a pump photon to a Stokes photon and a pump photon, while creating two phonons in the medium.

3.2 Modeling formalism for Raman wavelength converters

We consider a continuous-wave anti-Stokes Raman converter (see schematic representation of Figure 4(a)) where a strong pump input field and a weak Stokes input field enter a Raman-active medium and are as such subjected to the processes of SSRS, SARS and CARS. At the exit of the medium, the pump field is depleted and an increased Stokes field and anti-Stokes field emerge. To formulate the spatial propagation equations for the pump, Stokes and anti-Stokes fields in the converter, we rely on a susceptibility-based formalism that describes the SSRS, SARS, and CARS mechanisms by the use of the third-order Raman susceptibilities χ_{ss}, χ_{aa} and χ_{sa}, respectively.[1] We hereby remark that all mathematical formalisms used to describe these three processes are basically identical. Near Raman resonance, the Raman susceptibilities are of the form[1,11,12]

$$\chi_{\{ss,aa,sa\}} = \frac{-K_{\{ss,aa,sa\}}}{\omega_x - \omega_y - \omega_Q - i\Gamma} \tag{1}$$

where ω_x, ω_y represent pump, Stokes or anti-Stokes angular frequencies depending on the type of Raman transition, and where the involved oscillation energy level is characterized by a frequency ω_Q and by a linewidth Γ. For a non-inverted Raman medium, the functions $K_{\{ss,aa,sa\}}$ in Eq. (1) are real and positive.[1,11,12] When in addition the transitions are exactly at Raman resonance (i.e. $\omega_x - \omega_y = \omega_Q$), one finds that all Raman susceptibilities are negative imaginary and of the form $-iK_{\{ss,aa,sa\}}/\Gamma$.[1,11,12] If furthermore we assume that the real-valued non-resonant electronic susceptibility χ_{NR} of the Raman medium is negligible compared to $K_{\{ss,aa,sa\}}/\Gamma$, then the propagation equations for the complex pump field amplitude E_p, the complex Stokes field amplitude E_s, and the complex anti-Stokes field amplitude E_a, under the supposition that all three fields are monochromatic and that one can use the slowly varying amplitude approximation, are expressed as follows:[1,11,12]

$$\frac{\partial E_p}{\partial z} = G_p \left|E_a\right|^2 E_p - \frac{\omega_p n_s}{\omega_s n_p} G_s \left|E_s\right|^2 E_p \tag{2}$$

$$\frac{\partial E_s}{\partial z} = G_s \left|E_p\right|^2 E_s + \frac{\omega_s n_a}{\omega_a n_s} C_{sa} E_p^2 E_a^* e^{i\Delta kz} \tag{3}$$

$$\frac{\partial E_a}{\partial z} = -\frac{\omega_a n_p}{\omega_p n_a} G_p \left|E_p\right|^2 E_a - C_{sa} E_p^2 E_s^* e^{i\Delta kz} \tag{4}$$

Hereby,

$$G_s = \left[\left(2\pi\omega_s\right)/\left(cn_s\right)\right]\left(K_{ss}/\Gamma\right) \tag{5a}$$

$$G_p = \left[\left(2\pi\omega_p\right)/\left(cn_p\right)\right]\left(K_{aa}/\Gamma\right) \tag{5b}$$

$$C_{sa} = \left[\left(2\pi\omega_a\right)/\left(cn_a\right)\right]\left(K_{sa}/\Gamma\right) \tag{5c}$$

represent the SSRS-related Stokes gain coefficient, the SARS-related pump gain coefficient, and the CARS-related Stokes-anti-Stokes coupling coefficient, respectively (in Gaussian units). These three coefficients are all real and positive. Using the relation

$$\frac{\partial \left|E\right|^2}{\partial z} = \frac{\partial}{\partial z}\left(EE^*\right) = 2\,\mathrm{Re}\left(E^* \frac{\partial E}{\partial z}\right) \tag{6}$$

one can deduce from Eqs. (2)-(4) the following expressions:

$$\frac{1}{\hbar\omega_p}\frac{\partial\left|E_p\right|^2}{\partial z}=\frac{2}{\hbar\omega_p}G_p\left|E_a\right|^2\left|E_p\right|^2-\frac{2}{\hbar\omega_s}\frac{n_s}{n_p}G_s\left|E_s\right|^2\left|E_p\right|^2 \tag{7}$$

$$\frac{1}{\hbar\omega_s}\frac{\partial\left|E_s\right|^2}{\partial z}=\frac{2}{\hbar\omega_s}G_s\left|E_p\right|^2\left|E_s\right|^2+\frac{2}{\hbar\omega_a}\frac{n_a}{n_s}\mathrm{Re}\left(C_{sa}E_p^2E_a^*E_s^*e^{i\Delta kz}\right) \tag{8}$$

$$\frac{1}{\hbar\omega_a}\frac{\partial\left|E_a\right|^2}{\partial z}=-\frac{2}{\hbar\omega_p}\frac{n_p}{n_a}G_p\left|E_p\right|^2\left|E_a\right|^2-\frac{2}{\hbar\omega_a}\mathrm{Re}\left(C_{sa}E_p^2E_a^*E_s^*e^{i\Delta kz}\right) \tag{9}$$

When we assume that $n_a/n_s \approx 1$, we find that the last terms in Eqs. (8)-(9), i.e. the terms which represent the CARS contributions to the Stokes and anti-Stokes photon numbers, respectively, are exactly each other's opposite. This implies that in any infinitesimally small interval of the converter the sum of the generated Stokes and anti-Stokes photon numbers is not influenced by the CARS process. Since CARS does not influence the pump photon number either (see Eq. (7)), the only way that two pump photons, one Stokes photon and one anti-Stokes photon can participate in the CARS mechanism is according to the scheme of either Figure 3(a) or Figure 3(b). Due to the law of energy conservation, these two schemes are accompanied by phonon annihilation and phonon creation, respectively. Thus, although one often assumes that a four-wave mixing process can not exchange energy with the medium in which it takes place, we find that exactly at Raman resonance CARS does exchange energy with the medium. Furthermore, we conclude that, besides generating heat in the way that SSRS and SARS do, CARS can also extract heat from the Raman medium. This heat-extracting capability of CARS can be used e.g. for intrinsically mitigating the heat dissipation in Raman lasers,[14] as will be discussed further on in this paper.

To find out which of the two CARS schemes of Figures 3(a)/3(b) takes place along the fields' propagation path in the Raman converter, we need to determine at each position of the propagation path whether the opposite CARS contributions $+\left(2/\left(\hbar\omega_a\right)\right)\mathrm{Re}\left(C_{sa}E_p^2E_a^*E_s^*e^{i\Delta kz}\right)$ and $-\left(2/\left(\hbar\omega_a\right)\right)\mathrm{Re}\left(C_{sa}E_p^2E_a^*E_s^*e^{i\Delta kz}\right)$ to the Stokes and anti-Stokes photon numbers are respectively positive/negative-valued (the scheme of Figure 3(b) is valid) or negative/positive-valued (the scheme of Figure 3(a) is valid). Taking into account that $\hbar\omega_a$ and C_{sa} are real and positive constants, we thus need to find out in what way the sign of $\mathrm{Re}\left(E_p^2E_a^*E_s^*e^{i\Delta kz}\right)$ evolves during propagation in the converter. The function $\mathrm{Re}\left(E_p^2E_a^*E_s^*e^{i\Delta kz}\right)$, which actually represents a measure for the CARS-induced gain for the Stokes or anti-Stokes photons, will thus play a central role in our analysis of the CARS behavior, and we will from now on refer to it as the "CARS function".

We remark that the CARS function not only provides information on the CARS-induced photon growth, but also on the energy exchange between CARS and the Raman medium. Indeed, the CARS contribution to the material excitation magnitude $\left|\rho_{fi}\right|^2$ as defined by Y. R. Shen[1] is, in quasi-stationary regime, proportional to the CARS function $\mathrm{Re}\left(E_p^2E_a^*E_s^*e^{i\Delta kz}\right)$ with a proportionality constant that is real and positive.[1] Hence, a positive-valued CARS function not only implies that at that point CARS increases the number of Stokes photons at the expense of the anti-Stokes photons, but also that this photon interaction is accompanied by an excitation of the Raman medium or in other words by a creation of phonons. This finding is in full correspondence with Figure 3(b). A completely analogous reasoning can be made for a negative-valued CARS function, which corresponds to the interaction shown in Figure 3(a).

3.3 Analysis of the CARS behavior for different levels of pump depletion and phase mismatch values

To fix ideas, we first consider a hydrogen-based Raman converter with a considerable phase mismatch of Δk = 60 rad/m. We here choose hydrogen gas as Raman-active medium since it has negligible optical losses. Nevertheless, the findings presented in this Section will also be valid for Raman converters based on other Raman media such as SOI. Figures 4(b) and 4(c) show the spatial evolution along the hydrogen Raman converter of the pump, Stokes and anti-Stokes intensities and of the CARS function, as numerically obtained by solving Eqs. (2)-(4). The graphs in the undepleted pump region ($z \le z_d$) can also be calculated analytically[1,13] (see dotted lines in Figure 4). Using this analytic approach, we can show that the CARS function is negative for all $z \le z_d$ (see e.g. Figure 4(c)), and this for any value of the phase mismatch. In other words, in the converter propagation range where the pump depletion is negligible ($z \le z_d$), the CARS process, whatever the value of its phase mismatch, converts Stokes photons to anti-Stokes photons while annihilating phonons, along the scheme depicted in Figure 3(a). In the region where the pump gets depleted ($z > z_d$), we need to rely again on the numerically obtained curves. We can show that in this region the spatial evolution of the phase of the complex Stokes field amplitude slows down and eventually saturates (see Figure 4(d)) and that as a result the CARS function will evolve from negative values to positive values to finally converge to zero where $E_p \approx 0$, as can be seen in Figure 4(c).[13] Thus, when pump depletion occurs in combination with a considerable phase mismatch, the CARS process first converts Stokes photons to anti-Stokes photons while annihilating phonons (the scheme of Figure 3(a) is valid) and then switches over to the reverse process (the scheme of Figure 3(b) is valid).

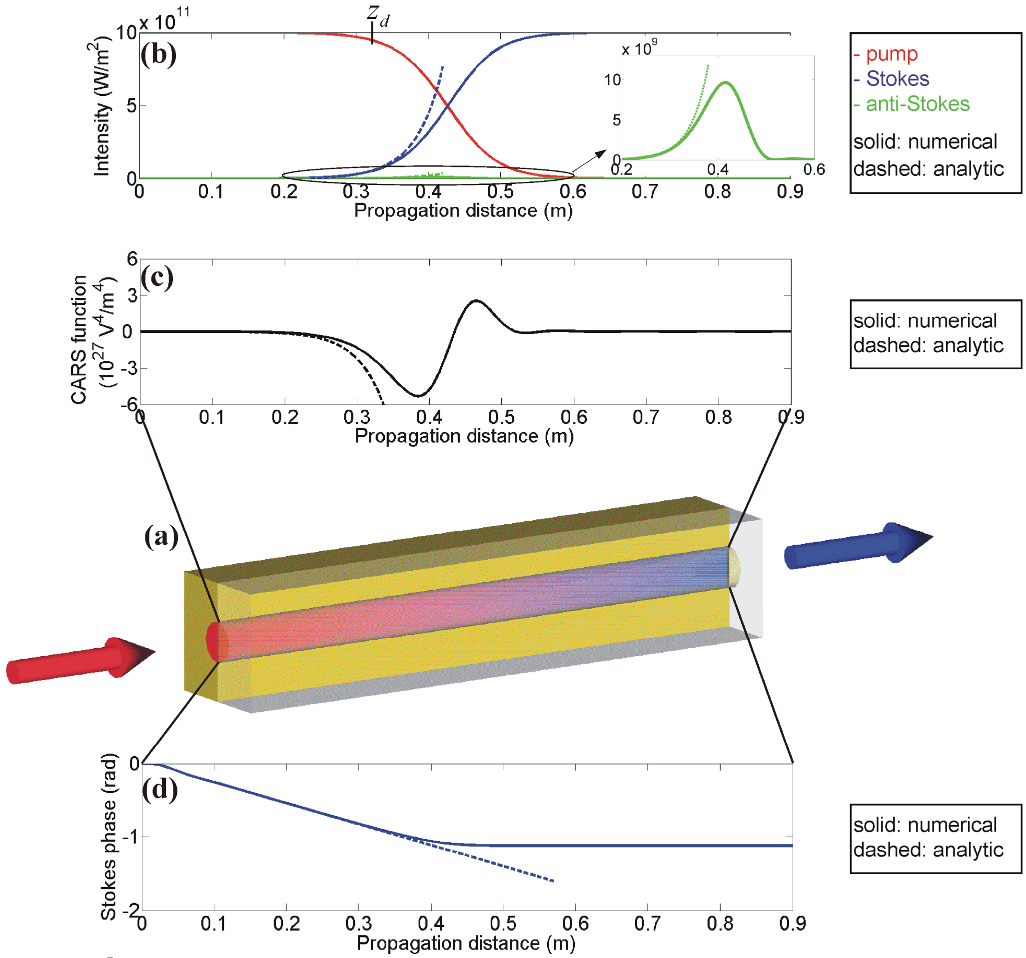

Fig. 4. Graphs associated with the first converter example featuring Δk= 60 rad/m. In (a), a cross-sectional schematic representation of the converter is shown, where a strong pump field (red) and a very small Stokes field (blue) are converted to a strong Stokes field (blue) and a weak anti-Stokes field (green). Graphs (b)-(d) show the spatial evolution along the converter of (b) the pump, Stokes and anti-Stokes intensities; (c) the CARS function; (d) the phase of the Stokes field amplitude. In these different graphs, the solid curves represent the numerically obtained results, whereas the dashed curves represent the analytic results valid in the region of negligible pump depletion

Next, we investigate what happens in case pump depletion occurs in a hydrogen-based Raman converter featuring a small phase mismatch of Δk=0.8 rad/m. In that case, we can show that when the pump depletion sets in, the phase evolution of the complex Stokes field amplitude will not immediately start to saturate.[13] The phase evolution will only begin to slow down when the pump is almost fully depleted ($E_p \approx 0$). Since only little pump power is left when the

Stokes phase saturation sets in, the propagation distance over which the initially negative-valued CARS function can increase again is too short to end up with a positive value for this function.[13] We thus find that CARS in case of pump depletion and quasi-perfect phase matching will continuously convert Stokes photons to anti-Stokes photons according to the scheme of Figure 3(a), without switching to the reverse interaction scheme of Figure 3(b).

3.4 Discussion

To interpret how exactly CARS generates anti-Stokes photons, most scientists have relied so far on the theory for phase-matched CARS that was launched in 1963 by Terhune.[15] The latter theory says that "the mechanism producing coherent anti-Stokes radiation *(i.e. CARS)* is a four-photon process during which two laser quanta are annihilated with the emission of a phase-matched Stokes and anti-Stokes quantum."[16] This interpretation of phase-matched CARS is schematically represented in Figure 5, and as can be seen in this Figure, it comprises no net energy exchange with the medium. From our derivations in Sec. 3.2 and 3.3 starting from the well established equations (2)-(4), we conclude that this model does not apply for phase-matched CARS at exact Raman resonance, since we have found that in that case CARS converts, regardless the level of pump depletion, a Stokes and a pump photon to an anti-Stokes and a pump photon while annihilating two phonons (see Figure 3(a)) – an interaction completely different from that described by Terhune (see Figure 5).

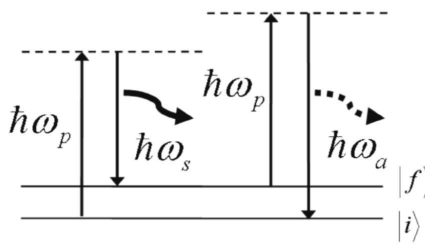

Fig. 5. Schematic representation of Terhune's interpretation of phase-matched CARS.

Over the past several decades, also other CARS theories have been introduced which are more in line with our model of CARS at exact Raman resonance. In 1963, Garmire, Pandarese and Townes[17] presented a theory for phase-matched CARS, which says that "Stokes radiation is initially produced *(via SSRS)* by maser light and subsequently anti-Stokes radiation is produced *(via CARS)* by the interaction of the maser light with the Stokes radiation, an interaction during which Stokes radiation is absorbed."[18] Next, our CARS model is to some extent supported by the theory[5,19] that Druet *et al.* presented in 1978-1981 based on earlier indications[20] from Bloembergen and by the model[11] that Bobbs and Warner introduced in 1990. Both the research teams of Druet *et al.* and of Bobbs and Warner also derived the two proper energy transfer schemes of CARS at exact Raman resonance. However, Druet *et al.* did not analyze how the CARS behavior evolves with interaction length in a Raman medium, whereas Bobbs and Warner stated that the two energy transfer types would continuously alternate along the fields' propagation path with a period determined by the phase mismatch, and this under all possible circumstances. The latter does not correspond to our findings that there is only one transition from the CARS scheme of Figure 3(a) to the CARS scheme of Figure 3(b) along the converter path length, and even none in case of negligible pump depletion or quasi-perfect phase matching.

Important to note is that in some anti-Stokes Raman conversion experiments the Stokes input wavelength is tuned, just like in CARS spectroscopy and microscopy experiments[21], towards the working point where the CARS-generated anti-Stokes signal is maximal.[7,8] Since for a random Stokes wavelength the anti-Stokes generation by CARS not only depends on $\mathrm{Im}(\chi_{sa})$ but also on $\mathrm{Re}(\chi_{sa})$ (and on the real-valued non-resonant susceptibility χ_{NR}), the preferred working point is there where $\left(\mathrm{Re}(\chi_{sa})+\chi_{NR}\right)^2+\left(\mathrm{Im}(\chi_{sa})\right)^2$ becomes maximal and is situated close to, but not exactly at Raman resonance.[21] As can be derived from Eqs. (2)-(4), CARS then becomes a combination of the 'phonon-exchanging' processes shown in Figures 3(a)/3(b) and of Terhune's 'phonon-conserving' process depicted in Figure 6 and its reverse.[5,11,19,20] The rate of the phonon-exchanging processes is determined by $\mathrm{Im}(\chi_{sa})$, whereas the rate of the phonon-conserving processes depends on $\mathrm{Re}(\chi_{sa})$ and χ_{NR}.[5,19]

Finally, we remark that our model for CARS in an anti-Stokes Raman converter operating at exact Raman resonance in fact also describes the CARS behavior in a Raman laser. Indeed, as mentioned earlier, the most common working point of a Raman laser is at exact Raman resonance. And if in addition to the SSRS lasing mechanism also CARS becomes significant in a Raman laser, the laser can be considered as an anti-Stokes Raman converter placed inside a resonator.

In conclusion, we have revealed the behavior of CARS in an anti-Stokes Raman converter operating at exact Raman resonance. We have found that the process behaves in a much more complex way than has been assumed thus far. Our CARS model not only deepens the fundamental understanding of this important Raman mechanism, but will also enable scientists and engineers to further optimize the design of anti-Stokes Raman converters and of other devices and techniques, the working principle of which is based on this unique Raman process.

The finding that CARS at exact Raman resonance exchanges energy with the Raman medium in which it takes place and is even able to extract energy from the medium, inspired us to investigate whether CARS could be used for reducing the heat dissipation in SOI Raman lasers. The results of our investigations will be presented in the next Section.

4. CARS-BASED HEAT MITIGATION IN SOI RAMAN LASERS

4.1 Introduction

An important issue when operating optically pumped lasers is the heat dissipation inside the active medium due to the quantum defect between the pump and the lasing wavelength. The resulting increase in temperature can have detrimental consequences for the laser performance, such as a decrease of the lasing efficiency and a deterioration of the lasing medium and/or the beam quality. Most of the conventional heat disposal techniques based on water cooling or on heat convection and conduction are not ideal from the point of view of downscaling the laser volume, preventing thermally induced refractive index changes, and in case of a solid medium, mitigating thermally induced stresses. We know for example that to thermally manage a waveguide laser with a certain pump and output power, the width of the waveguide device must be large enough so that the generated heat can be efficiently conducted into the surrounding air and/or the waveguide's substrate.[22] Compactness, however, plays an important role since a reduction of the laser dimensions may result in a much broader applicability in the domains of micro-, nano- and integrated optics and of photonics in general. Improving the thermal management in a laser medium is therefore key to a higher reliability and lifetime of the laser and/or a route to further laser miniaturization. To that aim, intrinsic heat mitigation mechanisms should be used that, instead of disposing of the heat when it has reached the outer surface of the active medium, minimize the heat generation already inside the medium.

In this Section, we present a novel intrinsic heat mitigation technique[14,23,24,25] for reducing the heat dissipation in Raman lasers, the lasing mechanism of which is based on SSRS. Like all laser sources, Raman lasers need to cope with unwanted internal heat generation due to the quantum defect between the pump and Stokes lasing wavelength (see Figure 1(a)). The intrinsic heat mitigation approach that we present here relies on CARS; a process that, as we have seen in Sec. 3, is able to extract heat from the Raman medium in which it takes place. Our technique is able to suppress the heat dissipation inside a Raman laser medium without deteriorating the lasing performance. We remark that the Stokes lasing efficiency will be affected to some extent, but this is compensated for by the generation of a second type of emission, i.e. anti-Stokes emission. We thus conclude that our so-called "CARS-based heat mitigation" could pave the way to a better stability and reliability of Raman lasers and/or to further miniaturization of these laser sources without compromising the lasers' performance.

Besides explaining the basic principle of our CARS-based heat mitigation technique, we will derive the mathematical expressions for the heat dissipation in Raman lasers and define a figure of merit for our heat reduction approach. Finally, we numerically demonstrate that for SOI waveguide Raman lasers one can obtain under certain pumping conditions a reduction of the heat dissipation of at least 35% by the use of CARS-based heat mitigation.

4.2 Basic principle of CARS-based heat mitigation

The novel heat mitigation technique that we present here relies on the interplay between the processes of SSRS, SARS and CARS inside the non-inverted Raman medium of a Raman laser (see Figure 6). We again consider the commonly used working point where the Raman transitions are at exact Raman resonance. As explained earlier, SSRS is the actual lasing mechanism of a Raman laser, which converts a pump photon into a lower energy Stokes lasing photon and a phonon, as shown in the upper part of Figure 6. The resulting heat generation is thus due to the pump-Stokes quantum defect, the magnitude of which corresponds to the Raman shift of the material (=15.6 THz in case of silicon). Next, CARS in case of exact Raman resonance and in case of (quasi-)perfect phase matching converts, as discussed in Sec. 3, a pump photon and a Stokes photon into a pump photon and an anti-Stokes photon, while annihilating two phonons. This process, which reduces the quantum-defect heating in the medium, is visualized in the middle part of Figure 6. We recall from Sec. 3 that in case of a considerable phase mismatch, also the “reverse” CARS interaction can take place, where anti-Stokes photons are converted back to Stokes photons and where phonons are created instead of being annihilated. Finally, SARS converts part of the CARS-created anti-Stokes photons back to pump photons as shown in the lower part of Figure 6. The heat that is generated during this process is due to the anti-Stokes–pump quantum defect, the magnitude of which also corresponds to the Raman shift.

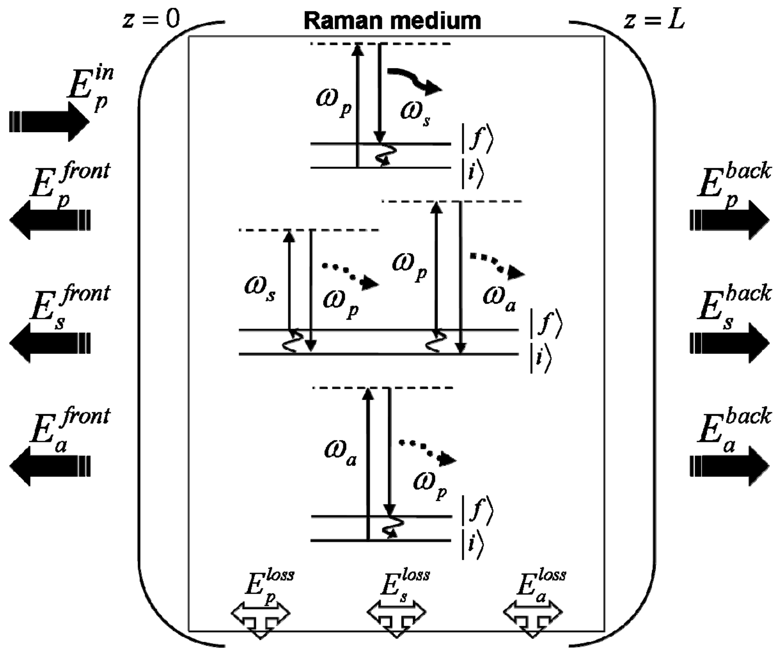

Fig. 6. Schematic representation of an optically pumped Raman laser with indication of the photon and phonon balances of SSRS (above), of CARS in case it converts Stokes photons to anti-Stokes photons (middle), and of SARS (below).

In case the actual Raman lasing mechanism, i.e. SSRS, is the only significant process in a Raman laser, the pump-Stokes quantum defect causes each generated Stokes lasing photon to be accompanied by a newly created phonon and as such to increase the heat dissipation in the Raman medium. However, when all three processes of SSRS, CARS and SARS are significant in a Raman laser, it becomes possible to create a given amount of Stokes lasing photons with less quantum-defect heating than the heating that would be generated in a SSRS-based Raman laser producing the same amount of Stokes lasing photons. The key to success here is the simultaneous generation of anti-Stokes photons through the CARS interaction as shown in Figure 6, during which phonons are annihilated. When we consider the photon and phonon balances of SSRS, CARS (both the interaction shown in Figure 6 and the reverse CARS interaction) and SARS, we find that the net amount of intra-cavity anti-Stokes photons, i.e. the amount that is not “absorbed” by SARS nor by the reverse CARS interaction, determines how many phonons are extracted from the Raman medium. On the other hand, the net amount of intra-cavity Stokes photons, i.e. the amount that is not “absorbed” by the CARS mechanism shown in Figure 6, indicates how many phonons are created in the medium. For a Raman laser in steady-state regime, the net amounts of Stokes and anti-Stokes photons generated inside the cavity are proportional to the numbers of Stokes and anti-Stokes photons coupled out of the cavity. We then find that the ratio of the number of out-coupled anti-Stokes photons to the number of out-coupled Stokes photons indicates how much the quantum-defect heating in the Raman laser is reduced with respect to the quantum-defect heating generated in a SSRS-based Raman laser that produces the same amount of Stokes photons. In other words, this photon number ratio corresponds to the ratio with which the average quantum-defect heating per out-coupled Stokes photon is reduced as compared to the quantum-defect heating per out-coupled Stokes photon in a SSRS-based Raman laser.

The basic idea behind the proposed intrinsic heat mitigation technique thus is to effectively mitigate the quantum-defect heating in a Raman laser by increasing the ratio of the number of out-coupled anti-Stokes photons to the number of out-coupled Stokes photons. We remark here that if we want to boost this ratio without deteriorating the actual laser output power (i.e. the Stokes output power), a large amount of anti-Stokes photons needs to be generated by CARS. The CARS process thus plays a very important role in the heat mitigation technique, hence the name "CARS-based heat mitigation".

To quantify the quantum-defect heating and the CARS-based heat mitigation efficiency in a Raman laser, we need a mathematical formalism that accurately describes the SSRS, CARS and SARS interactions in the Raman laser at exact Raman resonance. Hereto, we will use the Stokes–anti-Stokes iterative resonator method (IRM)[26,27,28] that we developed earlier on for modeling the operation of Raman lasers where all three Raman processes are significant.

4.3 Modeling formalism: Stokes–anti-Stokes IRM

To investigate the efficiency of CARS-based heat mitigation, we make use of the Stokes-anti-Stokes IRM that we developed, starting from the basic Raman propagation equations (2)-(4), for modeling continuous-wave Raman lasers.[26,27,28] This modeling method re-evaluates for every half round-trip time the longitudinal pump, Stokes and anti-Stokes electric field distributions inside the cavity until the steady-state regime is reached. Let us consider a Raman laser cavity with length L and with front and back mirror reflectivities $R_{\{p,s,a\},front}$ and $R_{\{p,s,a\},back}$ at the pump, Stokes, and anti-Stokes wavelengths $\lambda_p, \lambda_s, \lambda_a$, respectively. Applying for a certain half round-trip (α) the Stokes-anti-Stokes IRM to the amplitudes of the intra-cavity pump fields $E^+_{p,(\alpha)}(z)$ and $E^-_{p,(\alpha)}(z)$, Stokes fields $E^+_{s,(\alpha)}(z)$ and $E^-_{s,(\alpha)}(z)$, and anti-Stokes fields $E^+_{a,(\alpha)}(z)$ and $E^-_{a,(\alpha)}(z)$, propagating in the forward and the backward direction, respectively, yields the following equations:

$$\frac{\partial E^{\pm}_{p,(\alpha)}}{\partial z} = \left[\mp \frac{\omega_p}{\omega_s} \left(G^{\pm}_s \left| E^+_{s,(\alpha)} \right|^2 + G^{\mp}_s \left| E^-_{s,(\alpha)} \right|^2 \right) \right] E^{\pm}_{p,(\alpha)} + \left[\pm \left(G^{\pm}_p \left| E^+_{a,(\alpha)} \right|^2 + G^{\mp}_p \left| E^-_{a,(\alpha)} \right|^2 \right) \right] E^{\pm}_{p,(\alpha)} - \gamma^{\pm}_p E^{\pm}_{p,(\alpha)} \tag{10}$$

$$\frac{\partial E^{\pm}_{s,(\alpha)}}{\partial z} = \left[\pm \left(G^{\pm}_s \left| E^+_{p,(\alpha)} \right|^2 + G^{\mp}_s \left| E^-_{p,(\alpha)} \right|^2 \right) \right] E^{\pm}_{s,(\alpha)} \pm \left[\frac{\omega_s}{\omega_a} C_{sa} \left(E^{\pm}_{p,(\alpha)} \right)^2 \left(E^{\pm}_{a,(\alpha)} \right)^* F^{\pm} \right] - \gamma^{\pm}_s E^{\pm}_{s,(\alpha)} \tag{11}$$

$$\frac{\partial E^{\pm}_{a,(\alpha)}}{\partial z} = \left[\mp \frac{\omega_a}{\omega_p} \left(G^{\pm}_p \left| E^+_{p,(\alpha)} \right|^2 + G^{\mp}_p \left| E^-_{p,(\alpha)} \right|^2 \right) \right] E^{\pm}_{a,(\alpha)} \mp \left[C_{sa} \left(E^{\pm}_{p,(\alpha)} \right)^2 \left(E^{\pm}_{s,(\alpha)} \right)^* F^{\pm} \right] - \gamma^{\pm}_a E^{\pm}_{a,(\alpha)} \tag{12}$$

with $F^+ = e^{i\Delta k(\Lambda + z)}$ and $F^- = e^{i\Delta k(\Lambda + (L-z))}$ being the phase mismatch factors incorporating the influence of the CARS phase mismatch $\overrightarrow{\Delta k} = 2\overrightarrow{k_p} - \overrightarrow{k_s} - \overrightarrow{k_a}$. The factor z in F^+, F^- varies between $z = 0$ and $z = L$, whereas Λ equals the total distance that the fields have traversed inside the cavity over all previous half roundtrips. In Eqs. (10)-(12) we distinguish the Stokes and pump gain coefficients G^+_s, G^+_p for so-called "forward" SSRS and SARS (i.e. SSRS and SARS where the scattering occurs in the co-propagating direction) from the Stokes and pump gain coefficients G^-_s, G^-_p associated with so-called "backward" SSRS and SARS (i.e. SSRS and SARS taking place in the counter-propagating direction). These coefficients are defined as (SI units)

$$G^+_s = \frac{1}{4} \frac{g}{r^+} \left(\frac{\varepsilon_0}{\mu_0} \right)^{1/2} ; G^-_s = \frac{1}{4} \frac{g}{r^-} \left(\frac{\varepsilon_0}{\mu_0} \right)^{1/2} \tag{13}$$

$$G_p^+ = \frac{1}{4}\frac{\omega_p}{\omega_s}\frac{g}{r^+}\left(\frac{\varepsilon_0}{\mu_0}\right)^{1/2};G_p^- = \frac{1}{4}\frac{\omega_p}{\omega_s}\frac{g}{r^-}\left(\frac{\varepsilon_0}{\mu_0}\right)^{1/2} \tag{14}$$

As opposed to SSRS and SARS, CARS only takes place in the co-propagating direction, and the "forward" CARS-related coupling coefficient is given by (SI units)

$$C_{sa} = \frac{1}{4}\frac{\omega_a}{\omega_s}\frac{g}{r^+}\left(\frac{\varepsilon_0}{\mu_0}\right)^{1/2} \tag{15}$$

In Eqs. (13)-(15), g indicates the Raman gain constant, and $r^+, r^- (\geq 1)$ represent reduction coefficients for the efficiency of forward and backward Raman scattering, respectively. We can show that, in case of a pump linewidth $\Delta\nu_p$ within the limits set by dispersion,[29,30] the reduction coefficients r^+ and r^- are equal to 1 and $1+\Delta\nu_p/\Delta\nu_R$, respectively,[31] with $\Delta\nu_R$ representing the spontaneous Raman linewidth. We also remark that, apart from the reduction coefficients, the gain and coupling coefficients defined in Eqs. (13)-(15) correspond to those defined in Eqs. (5a)-(5c) and are only formulated in a different way: in Eqs. (13)-(15) we replaced the Raman susceptibilities by a Raman gain constant (while using the often employed approximation $\mathrm{Im}(\chi_{ss}) \approx \mathrm{Im}(\chi_{aa}) \approx \mathrm{Im}(\chi_{sa})$) and expressed the formulas in SI units instead of Gaussian units. $\gamma_p^\pm$, $\gamma_s^\pm$ and $\gamma_a^\pm$ in Eqs. (13)-(15) are the medium-dependent optical losses of the pump, Stokes and anti-Stokes fields, whereas the total power losses integrated over the cavity length at half round-trip (α) will be represented further on in this Section by the electric field amplitudes $E_{p,(\alpha)}^{loss}$, $E_{s,(\alpha)}^{loss}$, and $E_{a,(\alpha)}^{loss}$, respectively. We remark that these electric fields also contribute to the out-coupled photon numbers discussed earlier. Finally, the boundary conditions at the front and back cavity mirrors that link the successive half round-trips and the expressions for the field amplitudes $E_{\{p,s,a\},(\alpha)}^{\{front,back\}}$ emitted through the cavity mirrors can be found in our journal publication on the Stokes-anti-Stokes IRM[26], and will not be repeated here.

Now that we have defined a modeling formalism that allows us to further investigate the concept of CARS-based heat mitigation, we can mathematically quantify the quantum-defect heating in a Raman laser and the CARS-based heat mitigation efficiency.

4.4 Mathematical expressions for quantum-defect heating and for CARS-based heat mitigation efficiency

Using the modeling formalism described above, we can determine the total quantum-defect heating H at the half round-trip (α) by integrating the powers dP that are dissipated along the cavity over the cavity length L. Taking into account that $\frac{dP}{dz} = \mathrm{Re}\left(E^*\frac{dE}{dz}\right)\frac{A}{\mu_0 c}$ where A represents the modal effective area, we obtain that H for a Raman laser with significant SSRS, SARS and CARS, equals

$$\begin{aligned} H = \frac{A}{\mu_0 c}\Bigg\{&\int_{z=0}^{z=L}\sum_{\tau=+,-}\left[[1]_{(10),\tau}\left|E_{p,(\alpha)}^\tau\right|^2 - [1]_{(11),\tau}\left|E_{s,(\alpha)}^\tau\right|^2\right]dz \\ &+\int_{z=0}^{z=L}\sum_{\tau=+,-}\left[[1]_{(12),\tau}\left|E_{a,(\alpha)}^\tau\right|^2 - [2]_{(10),\tau}\left|E_{p,(\alpha)}^\tau\right|^2\right]dz \\ &+\int_{z=0}^{z=L}\sum_{\tau=+,-}\left[\mathrm{Re}\left([2]_{(12),\tau}\left(E_{a,(\alpha)}^\tau\right)^*\right) - \mathrm{Re}\left([2]_{(11),\tau}\left(E_{s,(\alpha)}^\tau\right)^*\right)\right]dz\Bigg\} \end{aligned} \tag{16}$$

Here, $[x]_{(y),\tau}$ indicates the x-th term in square brackets of equation (y), that corresponds to forward propagation if $\tau = +$ and to backward propagation if $\tau = -$. A good figure of merit for CARS-based heat mitigation is the ratio with which the average quantum-defect heating per out-coupled Stokes photon is reduced compared to the corresponding quantum-defect heating in a SSRS-based Raman laser. Assuming steady-state laser operation, we find that this figure of merit or "CARS-based heat mitigation efficiency" η_{HM} can be expressed as

$$\eta_{HM} = \frac{\left|E_{a,(\alpha)}^{front}\right|^2 + \left|E_{a,(\alpha)}^{back}\right|^2 + \left|E_{a,(\alpha)}^{loss}\right|^2}{\left|E_{s,(\alpha)}^{front}\right|^2 + \left|E_{s,(\alpha)}^{back}\right|^2 + \left|E_{s,(\alpha)}^{loss}\right|^2} \frac{\omega_s}{\omega_a} \times 100\% \tag{17}$$

Using the modeling formalism and the mathematical expressions introduced here, we are able now to numerically investigate the applicability of CARS-based heat mitigation to a concrete SOI waveguide Raman laser.

4.5 Application of CARS-based heat mitigation to a mid-infrared SOI waveguide Raman laser

In this Section, we will calculate the attainable CARS-based heat mitigation efficiency η_{HM} for a concrete SOI waveguide Raman laser. We remark that the heat mitigation technique should not compromise the Stokes lasing power, and therefore the Raman laser needs to generate many anti-Stokes photons to enhance η_{HM}. Firstly, one can strengthen the anti-Stokes generation through CARS by fulfilling the phase matching condition i.e. $\Delta k = 0$. Secondly, from the paragraph following Eqs. (13)-(15), we know that for pump linewidth values within the limits set by dispersion – these limits determine the pump linewidth values for which the pump field still coherently propagates with the Stokes and anti-Stokes fields but only in the copropagating scattering direction – the gain of backward Raman scattering will decrease with increasing pump linewidth whereas the gain of forward Raman scattering will remain unchanged. Thus, when increasing the pump linewidth, fewer anti-Stokes photons are "absorbed" by backward SARS, whereas the efficiencies of the forward SSRS lasing process and the CARS process does not decrease.

Let us now consider an SOI waveguide Raman laser operating in the mid-infrared wavelength region above 2.2 μm. Although mid-infrared emission from an SOI waveguide Raman laser has not been demonstrated yet, many research efforts are made to reach this goal soon.[32,33] The reason for considering here a silicon-based Raman laser operating in the mid-infrared rather than in the near-infrared telecom region is two-fold: on one hand, phase matching (i.e. $\Delta k = 0$) in an SOI waveguide can in practice be achieved more easily in the mid-infrared spectral region than in the near-infrared,[31] and, on the other hand, the strong nonlinear optical losses in silicon at near-infrared wavelengths, namely two-photon absorption (TPA) and TPA-induced free carrier absorption (FCA), do not occur for mid-infrared wavelengths beyond 2.2 μm.[32,34]

Let us assume that the SOI waveguide Raman laser under consideration is pumped by a continuous-wave mid-IR fiber laser featuring a pump wavelength λ_p = 2.7 μm, an output power of 5 W, and a relatively large pump linewidth $\Delta\nu_p$ = 300 GHz.[35] For a pump wavelength of 2.7 μm, we obtain that the Stokes and anti-Stokes wavelengths in the silicon-based Raman laser equal λ_s = 3.14 μm and λ_a = 2.37 μm. Since these wavelengths are larger than 2.2 μm, no TPA nor TPA-induced FCA will occur in the silicon medium. Taking into account that the Raman gain g scales approximately linearly with the pump frequency,[36] we obtain for the mid-infrared Raman laser a gain of g = 1.6×10^{-8} cm/W. The remaining parameter values of the Raman laser under study are: L = 2.5 cm, A = 3 μm^2, linear losses $\gamma_p^{\pm} = \gamma_s^{\pm} = \gamma_a^{\pm} = \pm 1$ dB/m, Δk = 0 cm^{-1}, spontaneous Raman linewidth $\Delta\nu_R$ = 215 GHz,[36] $R_{p,front} = R_{p,back}$ = 0.05, $R_{s,front} = R_{s,back}$ = 0.45, $R_{a,front} = R_{a,back}$ = 0. We also assume that no power is absorbed inside the cavity mirrors. We remark that these mirror reflectivities were chosen such that the corresponding simulation results clearly demonstrate the viability of CARS-based heat mitigation. The heat mitigation efficiency that we will obtain for these mirror reflectivities can also be achieved using other reflectivity sets. Since the calculations are computationally intensive, we did not perform an extensive numerical study of the reflectivities' influence on the heat mitigation efficiency and we consider in a first approach only the current set of reflectivity values.

When implementing the above mentioned parameter values in the Stokes-anti-Stokes IRM, we obtain the simulation results shown in Figure 7 for the evolution of the powers emitted through the front and back cavity mirrors versus the number of half round-trips. Here, we see that the emitted pump, Stokes and anti-Stokes powers evolve to steady-state values of 1.41 W, 0.69 W, and 0.43 W, respectively. To determine the CARS-based heat mitigation efficiency η_{HM} defined in Eq. (17), we need to calculate the total out-coupled Stokes and anti-Stokes photon numbers per half round-trip during the laser's steady-state regime. These numbers are obtained by summing the photon numbers that are emitted through the cavity mirrors (see Figure 7) and the amounts of photons that are coupled out or leaked out along the cavity via the linear losses. When calculating the ratio of the total number of out-coupled anti-Stokes photons to the total number of out-coupled Stokes photons, we obtain that the CARS-based heat mitigation efficiency η_{HM} equals 35%.[37,38] Furthermore, the quantum-defect heating H per half round-trip in the steady-state regime as defined in Eq. (16) equals 0.135 W, which is 7% of the converted pump power. We remark that since no additional heat generating mechanisms such as e.g. TPA or TPA-induced FCA are taking place in the mid-infrared SOI waveguide Raman laser, the obtained CARS-based heat mitigation efficiency immediately also indicates the ratio with which the overall heating in the laser is reduced.

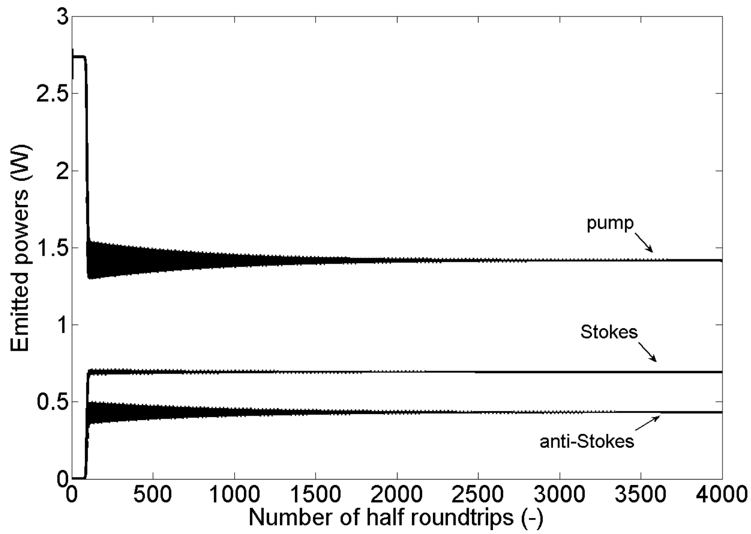

Fig. 7. Pump, Stokes and anti-Stokes powers emitted through the front and back cavity mirrors of a mid-infrared SOI waveguide Raman laser versus the number of fulfilled half round-trips.

In conclusion, we have introduced a novel intrinsic heat mitigation approach for Raman lasers, where CARS is used to suppress the heat dissipation in the laser medium. Furthermore, using the Stokes–anti-Stokes IRM we have numerically calculated that the CARS-based heat mitigation technique could reduce the heat dissipation in mid-infrared SOI waveguide Raman lasers with as much as 35%, which demonstrates the viability of our technique.

5. SUMMARY

In this paper, we have discussed the latest research results in the emerging field of CARS-based silicon photonics. With respect to CARS-based Raman wavelength converters in SOI technology, there has been much progress over the past few years regarding the conversion efficiency of these devices. Furthermore, by studying into detail the behavior of CARS in Raman wavelength converters, we have found that the process behaves in a much more complex way than has been assumed thus far and that it is able to extract heat from the Raman medium in which it takes places. Finally, based on the latter finding, we have conceptualized a novel technique that uses CARS to intrinsically reduce the heat dissipation in Raman lasers. Using an earlier developed modeling method for Raman laser sources, we have numerically demonstrated that this so-called "CARS-based heat mitigation technique" could suppress the heat generation in mid-infrared silicon-based Raman lasers with as much as 35%.

ACKNOWLEDGEMENTS

The work reported here is financially supported in part by FWO (Fonds voor Wetenschappelijk Onderzoek – Vlaanderen) that provides a Postdoctoraal Onderzoeker grant for N. Vermeulen and for C. Debaes, and in part by the EC 6th FP NEMO network, IAP BELSPO, VUB-GOA, and the OZR of the Vrije Universiteit Brussel.

REFERENCES

[1] Y. R. Shen, *[The Principles of Nonlinear Optics]*, Wiley-Interscience, USA, ch. 10 (2003).

[2] R. Claps, D. Dimitropoulos, V. Raghunathan, Y. Han, and B. Jalali, "Observation of stimulated Raman amplification in silicon waveguides," *Opt. Express* **11**, 1731-1739 (2003).

[3] O. Boyraz and B. Jalali, "Demonstration of a silicon Raman laser," *Opt. Express* **12**, 5269-5273 (2004).

[4] H. Rong, R. Jones, A. Liu, O. Cohen, D. Hak, A. Fang, and M. Paniccia, "A continuous-wave Raman silicon laser," *Nature* **433**,725-728 (2005).

[5] S. A. J. Druet and J. P. E. Taran, "CARS spectroscopy," *Prog. Quantum Electron.* **7**, 1-72 (1981).

[6] M. Muller, J. Squier, C. A. De Lange, and G. J. Brakenhoff, "CARS microscopy with folded BoxCARS phasematching," *J. Microsc-Oxford* **197**, 150-158 (2000).

[7] R. Claps, V. Raghunathan, D. Dimitropoulos, and B. Jalali, "Anti-Stokes Raman conversion in silicon waveguides," *Opt. Express* **11**, 2862-2872 (2003).

[8] V. Raghunathan, R. Claps, D. Dimitropouls, and B. Jalali, "Parametric Raman Wavelength Conversion in Scaled Silicon Waveguides," *J. Lightwave Technol.* **23**, 2094-2102 (2005).

[9] P. V. Koonath, D. R. Solli, and B. Jalali, "High Efficiency CARS Conversion in Silicon," *Conference on Lasers and Electro-Optics/Quantum Electronics and Laser Science Conference and Photonic Applications Systems Technologies*, paper CThE3 (2008).

[10] K. K. Tsia, S. Fathpour, and B. Jalali, "Electrical tuning of birefringence in silicon waveguides," *Appl. Phys. Lett.* **92**, 061109 (2008).

[11] B. Bobbs and C. Warner, "Raman-resonant four-wave mixing and energy transfer," *J. Opt. Soc. Am. B* **7**, 234-238 (1990).

[12] R. W. Boyd, *[Nonlinear Optics - Second Edition]*, Academic Press, USA, ch. 10 (2003).

[13] N. Vermeulen, C. Debaes, and H. Thienpont, "The behavior of CARS in anti-Stokes Raman converters operating at exact Raman resonance," *IEEE J. Quantum Electron.* **44**, 1248-1255 (2008).

[14] N. Vermeulen, C. Debaes, P. Muys, and H. Thienpont, "Mitigating heat dissipation in Raman lasers using Coherent Anti-Stokes Raman Scattering," *Phys. Rev. Lett.* **99**, 093903 (2007).

[15] R.W. Terhune, "Nonlinear Optics," *Bull. Am. Phys. Soc.* **8**, 359 (1963).

[16] H. J. Zeiger, P. E. Tannenwald, S. Kern, and R. Herendeen, "Two-step Raman scattering in nitrobenzene," *Phys. Rev. Lett.* **11**, 419-422 (1963).

[17] E. Garmire, F. Pandarese, and C. H. Townes, "Coherently driven molecular vibrations and light modulation," *Phys. Rev. Lett.* **11**, 160-163 (1963).

[18] R. Chiao and B. P. Stoicheff, "Angular dependence of maser-stimulated Raman radiation in calcite," *Phys. Rev. Lett.* **12**, 290-293 (1964).

[19] S. A. J. Druet, B. Attal, T. K. Gustafson, and J. P. Taran, "Electronic resonance enhancement of coherent anti-Stokes Raman scattering," *Phys. Rev. A* **18**, 1529-1557 (1978).

[20] N. Bloembergen, *[Nonlinear Optics]*, W. A. Benjamin, USA, ch. 2 (1965).

[21] A. Penzkofer, A. Laubereau and W. Kaiser, "High intensity Raman interactions," *Prog. Quantum Electron.* **6**, 55-140 (1979).

[22] D. P. Shepherd, S. J. Hettrick, C. Li, J. I. Mackenzie, R. J. Beach, S. C. Mitchell, and H. E. Meissner, "High-power planar dielectric waveguide lasers," *J. Phys. D: Appl. Phys.* **34**, 2420-2432 (2001).

[23] N. Vermeulen, C. Debaes, and H. Thienpont, "Cooling silicon Raman lasers using Coherent Anti-Stokes Raman Scattering (CARS)," *Optical Society of America (OSA) Opt. Photonics News* **18** (special edition "Optics in 2007"), 24 (2007).

[24] N. Vermeulen, C. Debaes, and H. Thienpont, "Optical cooling of Raman lasers using CARS," *Proc. SPIE* **6461**, 64610D (2007).

[25] N. Vermeulen, C. Debaes, and H. Thienpont, "Mitigating heat dissipation in a hydrogen-based Raman laser using Coherent Anti-Stokes Raman Scattering," *Proc. SPIE* **6582**, 65820W (2007).

[26] N. Vermeulen, C. Debaes, A. A. Fotiadi, K. Panajotov, and H. Thienpont, "Stokes-anti-Stokes iterative resonator method for modeling Raman lasers," *IEEE J. Quantum Electron.* **42**, 1144-1156 (2006).

[27] N. Vermeulen, A.A. Fotiadi, C. Debaes, K. Panajotov, and H. Thienpont, "Iterative resonator model describing the continuous-wave operation of a Raman laser," *Proc. SPIE*. **6190**, 61900Q (2006).

[28] N. Vermeulen, C. Debaes, and H. Thienpont, "Iterative resonator model describing the Stokes and anti-Stokes emission of a continuous-wave silicon-based Raman laser," *Proc. SPIE*. **6455**, 64550N (2007).

[29] W. R. Trutna, Y. K. Park, and R. L. Byer, "The Dependence of Raman Gain on Pump Laser Bandwidth," *IEEE J. Quantum Electron.* **15**, 648-655 (1979).
[30] K. Sentrayan, A. Michael, and V. Kushawaha, "Intense backward Raman lasers in CH_4 and H_2," *Appl. Opt.* **32**, 930-934 (1993).
[31] N. Vermeulen, C. Debaes, and H. Thienpont, "Mitigating heat dissipation in near- and mid-infrared silicon-based Raman lasers using CARS – Part I: Theoretical analysis," *IEEE J. Sel. Top. Quantum Electron.* **13**, 770-782 (2007).
[32] V. Raghunathan, D. Borlaug, R. R. Rice, and B. Jalali, "Demonstration of a mid-infrared silicon Raman amplifier," *Opt. Express* **15**, 14355-14362 (2007).
[33] H. Rong, S. Xu, O. Cohen, O. Raday, M. Lee, V. Sih, and M. Paniccia, "A cascaded silicon Raman laser," *Nat. Phot.***2**, 170-174 (2008).
[34] N. Vermeulen, C. Debaes, and H. Thienpont, "Modeling mid-infrared continuous-wave silicon-based Raman lasers," *Proc. SPIE* **6455**, 64550U (2007).
[35] X. Zhu and R. Jain, "Numerical analysis and experimental results of high-power Er/Pr:ZBLAN 2.7 μm fiber lasers with different pumping designs," *Appl. Opt.* **45**, 7118-7125 (2006).
[36] L. Pavesi, D. J. Lockwood (Eds.), *[Silicon Photonics]*, Springer-Verlag, Germany, 209-220 (2004).
[37] N. Vermeulen, C. Debaes, and H. Thienpont, "Mitigating heat dissipation in near- and mid-infrared silicon-based Raman lasers using CARS – Part II: Numerical demonstration," *IEEE J. Sel. Top. Quantum Electron.* **13**, 783-788 (2007).
[38] N. Vermeulen, C. Debaes, and H. Thienpont, "Enhancement methods for CARS-based heat mitigation and application to near- and mid-infrared silicon-based Raman lasers," *Proc. SPIE* **6582**, 65820X (2007).